

catch the light

technical reprint R/P099



fast timing with inorganic
scintillators

fast timing with inorganic scintillators

A G Wright, Electron Tubes Ltd., Bury Street, Ruislip, HA4 7TA, UK

technical reprint R/P099

1 introduction

There are certain photomultiplier applications in which knowledge of the time of occurrence of each event is required. For example: time of flight in neutron spectroscopy and general timing experiments with scintillators operated in coincidence. Currently, there is considerable interest in the use of massive gamma-ray-detectors in the search for illicit explosives (part of the "US homeland security" program). Some detectors are based on fast plastic scintillators, others use the relatively slow inorganic scintillators such as NaI(Tl) . This study concentrates on the latter.

The earliest consideration on timing was the seminal paper by Post and Shiff [1] in 1950; occupying just a single page and yet of considerable importance! The statistical treatment in [1] refers to light emission only, and takes no account of the influence of the photomultiplier (pmt) and associated electronics. Certain parameters must be introduced in order to fully understand the timing characteristics of any scintillation detector (see glossary of terms given in Appendix 1). We need to characterise the single-electron response and the transit-time jitter, \mathcal{E}_{ph} , of the pmt. The single-electron response, as the term implies, is the time and amplitude signature of a signal initiated by a single photoelectron. This is a statistical quantity, where both the shape and the area under the pulse fluctuate from one pulse to the next. In this study we investigate the effect of, \mathcal{E}_A , which represents the dispersion in the total charge generated per photoelectron. In fact, \mathcal{E}_A , is nothing other than the noise in the photomultiplier gain, g . Detailed coverage of the subject of timing with scintillators was given particular attention during the 1960s, with much of the work originating from Gatti and his colleagues [2], [3], and [4]. It was at this time that digital computers became more readily available for making Monte Carlo calculations and these studies [2] – [4] only became possible with the facility to perform random-number simulations. Hyman et al [5] carried out such simulations providing examples of anode pulse shapes for small numbers of photoelectrons, showing, perhaps for the first time, the

effects of statistical fluctuations. Their theoretical treatment provided timing predictions for fast scintillators. Gatti [4] published a review of theories and experiments on resolving time in 1966, summarising the work up to this date very effectively. In 1967 Gedcke and McDonald [6] introduced the Constant Fraction (CF) discriminator, which revolutionised the art of fast timing. It is unfortunate that the review article [4] just predates the introduction of what was to become standard electronics for fast timing.

The technical literature is predominantly directed at fast scintillators, but here we are interested in optimising the performance of slow scintillators, especially for those signals poorly endowed with photons. This, the first of two technical notes, concentrates on the slower inorganic scintillators. A second note on the performance of faster scintillators, such as plastic, is reserved for a later publication. The statistical arguments are the same in both cases, but the contribution from the pmt is more significant with fast scintillators. For our purposes, a slow scintillator is one for which the decay time, τ , is much longer than all of the timing parameters that characterise the pmt. That is, $\tau \gg t_r, t_{fwhm}, \mathcal{E}_{ph}$ where t_r is the rise time and t_{fwhm} is the width of the characteristic single-electron response of the pmt. The jitter, \mathcal{E}_{ph} , of a pmt is defined as the variation in the transit-time from photocathode to anode for single photoelectron-initiated signals. In general, all three timing parameters have the same order of magnitude for a given pmt type: 1 – 2 ns for fast pmts with a linear focus dynode structure; up to 10 ns for the slower box-and-grid structures.

The aim of this technical paper is: to present the statistical arguments of timing in a way that experimental physicists and engineers can understand, and then use for their purposes; to use the statistical formulations to predict the upper limit to timing precision, based on photon arrival statistics alone; and finally, to predict the performance with a real photomultiplier when used with a constant fraction discriminator.

2 time distribution $P(Q,R,\tau,t)$ of photons emitted by a scintillator

There is a wide range of commercially available scintillators. Each may be characterised by a light output time profile, $f(t)$, with a total light output of R photons. The fastest scintillators, the organics, are characterised by decay times, τ , measured in nanoseconds, whilst in the inorganic scintillators,

such as $NaI(Tl)$ and BGO , the decay of the light output occurs over microseconds. R ranges from 10 to 50 photons per keV energy deposited respectively, for the two groups of scintillator. We will see that timing fidelity improves with increasing R and decreasing τ .

The distribution $P(Q,R,\tau,t)$, for a scintillator of decay time τ , gives the time of emission, t , of the Q th photon out of R and was derived by Post and Shiff [1] in 1950. They presented a general expression for $P(Q,R,\tau,t)$ that may be applied to any well-behaved function $f(t)$. They also provide an expression for the variance of $P(Q,R,\tau,t)$ for the special case of an exponential decay with a single time-constant. In this technical note we will also take $f(t)$ to be a decaying exponential with a single time-constant. For convenience of presentation, where appropriate, we sometimes substitute τ by $1/\lambda$ in the formulae. Light output from the scintillator is described by:

$$f'(t) = \frac{dQ(t)}{dt} = R \lambda \exp(-\lambda t) \quad \dots(1)$$

We restrict ourselves to small area and small volume scintillators and it therefore follows that the emission of a photon and its detection at the photocathode may be assumed isochronous. Integrating (1) from $t = 0$ to ∞ gives R , the total light output, as it must. $Q(t)$, the number of photons emitted from 0 to t , follows from integrating (1).

$$f(t) = Q(t) = R(1-\exp(-\lambda t)) \quad \dots(2)$$

The mean arrival time of the Q th photon is

$$t_Q = \tau \ln(R/(R-Q)) \quad \dots(3)$$

$$\approx Q/(\lambda R) (1 + Q/(2R)) \text{ for } Q \ll R$$

Equations (1) - (3) describe the average emission of light from a scintillator. This is illustrated in **figure 1** where emission times for a total of $R = 100$ photons are plotted using (2). The points fall on a smooth curve, but we note that time intervals between emissions increase with t , strictly in accordance with (2), of course. The concept of average in describing light emission from scintillators limits our ability to describe actual processes occurring in nature. Light emission from a scintillator, following excitation by a gamma-ray, for example, is a statistical process and we need to apply Monte Carlo methods to simulate real processes (see Appendix 2).

The statistical simulation of (2) is shown in **figure 1** where the random walk of the emission times around the path of (2) is very nicely illustrated (see Appendix 3 for further discussion).

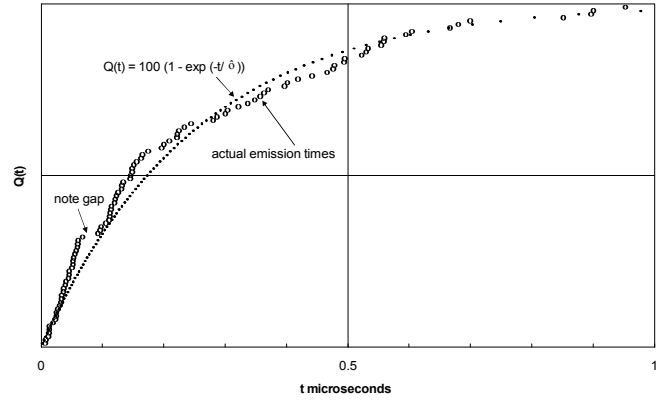


figure 1 illustrating the emission of photons from a scintillator with a single decay time-constant, τ . The small dots describe what would be obtained by averaging several hundred decay events, all of the same energy. The intervals between these dots increase with time in accordance with the exponential distribution. Any one particular event will follow a random path, such as that shown by circles.

The probability distribution, for the arrival of the Q th photon, at a time between t and $t + dt$, is best envisaged as a three-part process.

$$P_I(Q,R,\lambda,t) = p_a \cdot p_b \cdot p_c$$

where

- p_a = probability that $Q-1$ photons arrive within 0 and t
- p_b = probability that the Q th photon arrives between t and $t + dt$
- p_c = probability that $R-Q$ photons (the remainder) arrive after $t + dt$

where we have assumed that R is fixed (no statistical fluctuation). This is of restricted utility, but the general case will be developed later.

$$p_a = C(R,Q-1) \cdot \left\{ \int_0^t \lambda e^{-\lambda t} dt \right\}^{Q-1}$$

$$p_b = C(R-(Q-1),1) \lambda e^{-\lambda t} dt$$

$$p_c = \left\{ \int_t^\infty e^{-\lambda t} dt \right\}^{R-Q}$$

where $C(R,Q-1)$ is the number of combinations of R taken $Q-1$ at a time and $C(R-(Q-1),1)$ is the number of combinations of $R-(Q-1)$ taken 1 at a time, giving

$$\begin{aligned} P_I(Q,R,\lambda,t) &= \frac{R!(1-e^{-\lambda t})^{Q-1} (R-(Q-1)) \lambda e^{-\lambda t} dt (e^{-\lambda t})^{R-Q}}{(Q-1)!(R-(Q-1))!} \\ &= \frac{R! \lambda (1-e^{-\lambda t})^{Q-1} e^{-\lambda(R-Q+1)t} dt}{(Q-1)!(R-Q)!} \quad \dots(4) \end{aligned}$$

where $P_1(Q, E, \lambda, t)$ refers to fixed R , as stated earlier. We can derive an expression for the case in which R is taken as the mean of a Poisson distribution $p(n) = R^n e^{-R} / n!$. We include $p(n)$ in (4), thus

$$P_2(Q, R, \lambda, t) = \sum_Q^{\infty} p(n) \cdot P_1(Q, R, \lambda, t)$$

which leads to

$$P_2(Q, R, \lambda, t) = \frac{R^Q \lambda}{(Q-1)!} \exp(-R(1 - e^{-\lambda t})) \cdot (1 - e^{-\lambda t})^{Q-1} e^{-\lambda t} dt \quad \dots(5)$$

Equation (5) follows from Post and Shiff's formulation by substituting $f(t) = R(1 - \exp(-\lambda t))$ into their equations (1) and (2) [1]. Equation (5) is a particular solution for an exponential decay. Post and Shiff, however, provide an expression that may be applied to any well-behaved function $f(t)$ (this generality is quite extraordinary!). In a recent paper, Ranucci [7] derives the generalised formulations of (4) and (5), in an easy to follow way. This paper [7] is particularly recommended to the reader who is seeking a clear step-by-step derivation of the Post and Shiff formulae for the generalised stimulus, $f(t)$. In a way, the application of [1] to pulse shape discrimination (psd) in [7] is complimentary to timing: psd is concerned with the tail end of a scintillation pulse; timing depends on the leading edge of a pulse.

The time distribution for the arrival of the first photon is readily obtained by putting $Q = 1$ in (5) and if we take $\lambda t \ll 1$, then

$$P_2(1, R, \lambda, t) \approx R \lambda \exp(-(R+1)\lambda t) dt \quad \dots(6)$$

The result from (4) is the same, except that the argument in the exponential term is $-R\lambda t$. The distribution for the arrival of the first photon is very narrow compared with that of the emission spectrum. We see that it goes as $\sim \exp(-(R+1)\lambda t)$ compared with $\exp(-\lambda t)$ of the stimulus. This led to the statement in [1] that the best timing for any exponential decay process is obtained by recording the arrival of the first photon or photoelectron. Distributions for (4) and (5) are given in **figure 2(a)** and (b) for $R = 10$ and $R = 100$, respectively.

We note that the curves predicted by (4) and (5) are very similar provided that $Q \ll R$. For R large, say >1000 , the statistical fluctuation in R , that is $\sigma(R)/R$, is only $\sim 3\%$ and hence R is effectively fixed and (4) and (5) converge in their predictions. We take advantage of this and use (4) in preference to (5) which is particularly unwieldy through its dependence on $\exp(-R(1 - e^{-\lambda t}))$ – this presents diffi-

culties in any mathematical manipulation involving integration.

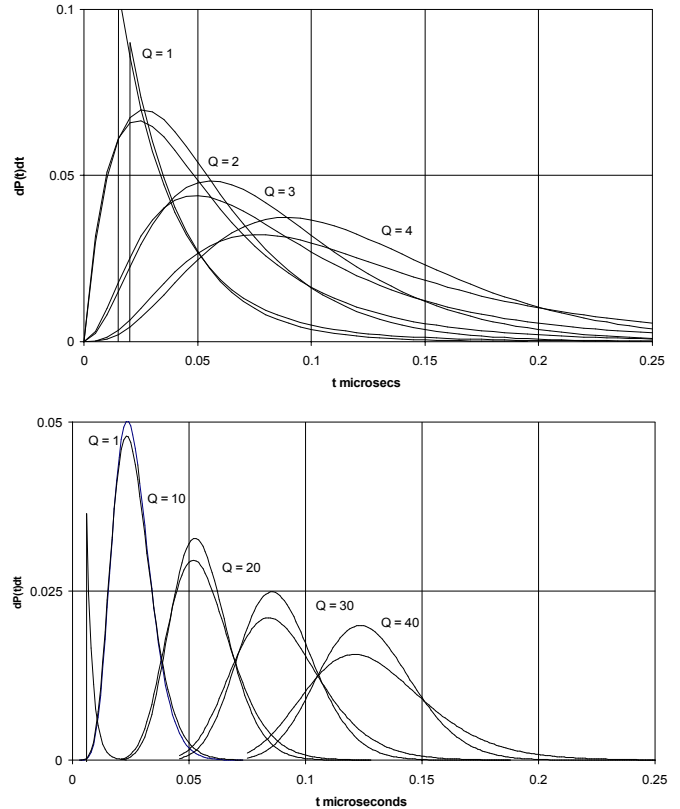


figure 2 a) timing distributions for the arrival of the first, second, third, and fourth photoelectrons in the decay of $NaI(Tl)$, $R = 10$, $\tau = 250$ ns. Solid curves refer to equation (5) while the dashed curves are for R fixed, equation (4). In b), $R = 100$ for the Q values indicated.

So far, we have been concerned with photon distributions, whereas we really want to know about photoelectron time distributions. Photocathode quantum efficiencies are typically $\sim 25\%$ for scintillators that emit in the blue region of the spectrum and we must scale R appropriately to deduce the number of photoelectrons. The same statistics still apply, however, because, although photoelectron emission is governed by binomial statistics, the convolution of a Poisson distribution with a binomial always results in a Poisson [8]. Our initial assumption concerning the statistics of photoemission is valid for photoelectron emission and we may therefore consider all formulae to apply equally to photoelectrons.

3 the variance of $P(Q, R, \tau, t)$

The curves of **figure 2** provide complete information about the distribution of time intervals. However, we want a single parameter to characterise these curves, and $var(Q)$, the variance of $P(Q, R, \tau, t)$, provides this (where necessary a subscript will be used to indicate whether P_1 or P_2 is under consideration). The actual figure-of-merit we use to quantify timing dispersion is $\sigma(Q) = var^{1/2}(Q)$,

which has the dimension of time. The relationship in (7) is the variance of (5), and this has been taken from [1]. The derivation is complicated, requiring the use of generating functions and asymptotic expansions and will not be detailed here. According to [1], we have subject to $R \gg 1$ and $R \gg Q$:

$$\text{var}_2(Q) = \frac{Q}{R^2 \lambda^2} (1 + 2(1 + Q)/R + \dots) \quad \dots(7)$$

There is no indication in [1] as to the accuracy of (7) for any given R and Q , but we can, however, confirm more precisely the regions of validity of (7), with regard to R and Q , by actually calculating the variance of the distributions shown in figures 2(a) and (b) for comparison with (7). Since (5) is exact, it therefore offers a means of determining the variance without error by direct computation. These calculated variances are then compared with (7). The result of doing this is shown in figure 3 for $R = 100$. It is obvious for practical purposes that (7) is sufficiently accurate provided that $Q/R < 20\%$, and is useful even beyond these limits.

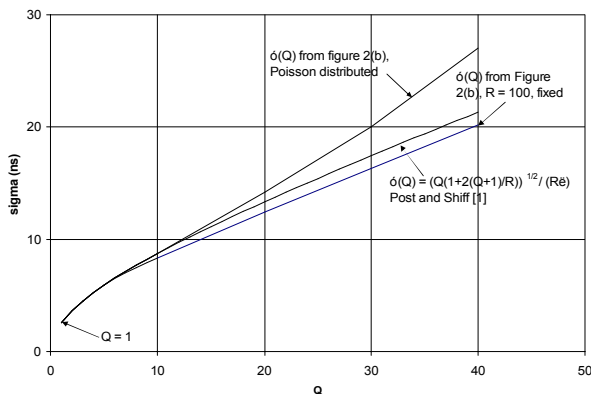


figure 3 $\sigma(Q)$ calculated from the distributions of figure 2(b), with $R = 100$ and $\tau = 0.25 \mu\text{s}$, shown together with the predictions of equation (7). The true dispersion is derived from the curves in figure 2(b) assuming a Poisson distribution for R . We note, however, that there is particularly good agreement for $Q < 10$, for all three considerations, and acceptable agreement up to $Q \sim 30$.

Having established the range of validity of (7), what then are the practical implications, noting from (7) that photoelectron time dispersion

$$\sigma_2(Q) \text{ varies as } Q^{1/2} \tau / R.$$

- best timing is obtained at the lowest thresholds of Q
- $\sigma(Q)$ varies only as $Q^{1/2}$
- $\sigma(Q)$ varies as τ , the scintillator time-constant
- $\sigma(Q)$ varies inversely with R , the number of photoelectrons in the decay

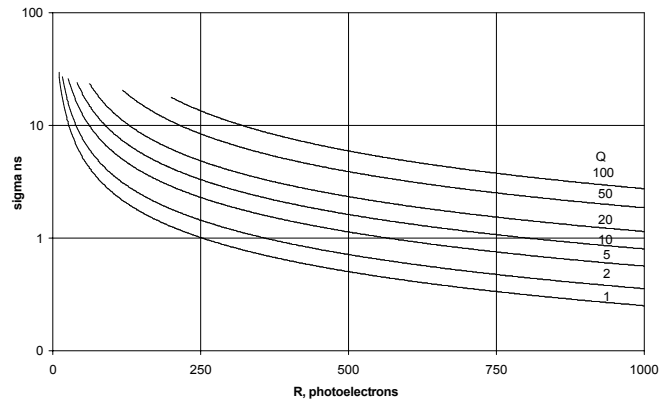


figure 4 the time dispersion, $\sigma(Q)$, for photoelectrons from NaI(Tl) , for a range of Q values.

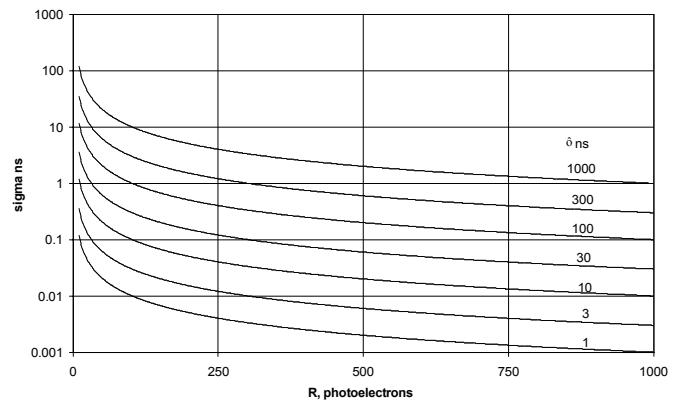


figure 5 the time dispersion for the first photoelectron from scintillators with decay times ranging from 1 ns to 1 μs .

4 the effect of photomultiplier transit time jitter, ϵ_{ph}

So far, we have only considered statistical effects that take place at the photocathode, but now we must include the contribution from the entire pmt. Each photoelectron produces a charge pulse at the anode, but delayed by the transit-time through the pmt. There are two contributions to transit-time dispersion. The first arises from the different paths taken by photoelectrons in traversing the cathode to first dynode region ($k - d_1$). The path taken, and hence the $k - d_1$ transit-time, depends on the point of initiation on the photocathode. In most pmts, photoelectrons with starting points near the perimeter of the cathode take an additional time, Δt_{k-d1} , to reach d_1 compared with those initiated close to the axis of the pmt. Δt_{k-d1} ranges from ~ 0.5 ns for a fast pmt [9], such as the 9954B, to ~ 5 ns for a 5 inch pmt with a plano-planar window (9330B). There is also a contribution to Δt_{k-d1} related to the angle of emission and the initial energy of each photoelectron, both of which are statistical in nature. The multiplier makes the second contribution, once again because of the various paths taken by the secondary electrons – the initial electron energies also play a part. The net effect is a transit-time dispersion ranging from ~ 1 ns in the fastest

pmts to ~ 10 ns in the slowest. The central limit theorem tells us that because \mathcal{E}_{ph} is produced by the cumulative effect of many independent variables (there are typically 10 to 14 dynodes in a pmt), the time dispersion will assume a normal distribution no matter what the distribution of the component variables may have been.

Monte Carlo simulations were run to select photoelectron emission times in accordance with (1) using the method in Appendix 2. To simulate the action of the multiplier, each photoelectron arrival time at the anode was randomised in accordance with a normal distribution characterised by (μ, σ_n) , where μ is the mean transit-time. The value of μ is arbitrary and the only requirement is that $\mu > 5\sigma_n$ to ensure only positive transit-times. σ_n was taken successively as 1, 2.5, and 5 ns to cover a range of pmt types. The arrival times at the anode were then sorted in ascending order to provide the time signature of an R -photoelectron event. This is shown in **figure 6(a)** for 100-photoelectron events and we note a small loss of timing resolution at low Q values because of \mathcal{E}_{ph} . **Figures 6(b)** and **(c)** apply to higher R -values and they show an even more pronounced loss in relative performance than is evident in (a). Referring to (c), the significant revelation in these curves is the improvement that can be gained by raising the detection threshold for optimum timing to $Q/R \sim 1\%$ or equivalently $Q = 50$ photoelectrons.

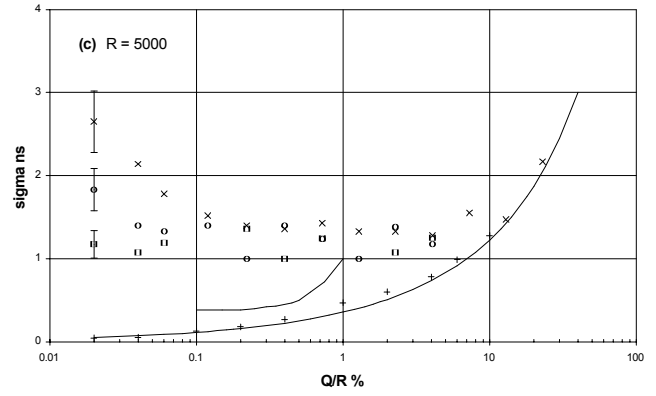
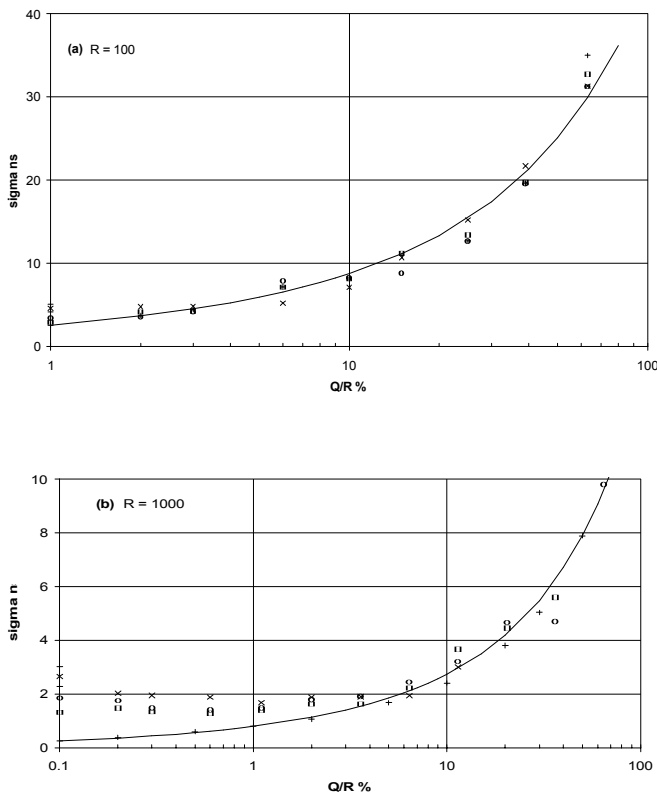


figure 6 $\sigma(Q)$ determined directly from (5), + , with the predictions of [1], solid line, for (a) $R = 100$, (b) $R = 1000$ and (c) $R = 5000$. The timing fidelity is impaired once transit time jitter is introduced. \square : $\mathcal{E}_{ph} = 1$ ns ; \circ : $\mathcal{E}_{ph} = 2.5$ ns; \times : $\mathcal{E}_{ph} = 5$ ns. The sporadic error bars give an indication of the precision. Measurements from [10] are shown by the dashed line.

Experimental results of Nutt et al [10] taken with a constant fraction discriminator are also shown in **figure 6(c)** for comparison. The energy is 511 keV equivalent to ~ 5000 photoelectrons and the results are compatible with theory. In another measurement [11] the transit-time dispersion was measured as 0.34 ns for ^{60}Co and 0.55 ns for 511 keV. These results are also compatible with theory, but there is uncertainty in deducing the mean Q value that applies, and hence corresponding uncertainty in locating the measurements on the time axis.

5 the effect of noisy gain

It is well known that the gain capability of pmts is high, but as with all amplifiers, it is noisy. The single-electron response (SER) of a pmt characterises this noise: the SER is the pulse height distribution for anode signals initiated by single photons. The distribution is readily measured with a charge-sensitive, multi-channel analyser as shown in **figure 7(b)**. The mean of the distribution is taken as one photoelectron equivalent. A noiseless multiplier is one characterised by a δ -function response, such as (a), but in practice such a sharp response is never observed in conventional pmts. A noisy multiplier is represented by the exponential distribution of (c). We define a noise factor, NF , as

$$NF = [1 + \mathcal{E}_A]^{1/2} \quad \dots(8)$$

where $\mathcal{E}_A = \text{var}(h)/\langle h \rangle^2$, represents the gain dispersion, which can be calculated directed from the SER. In the treatment so far we have assumed the gain is fixed, whereas it varies from pulse to pulse in accordance with (8). This assumption is removed when we consider practical timing circuits in section 8.

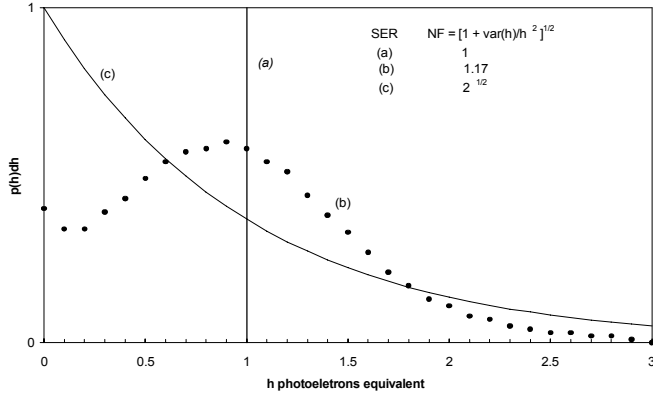


figure 7 pmt single-electron response curves, SER (a) noiseless gain (b) an SER representative of pmts with linear focus dynodes. (c) an exponential response describing the behaviour of Venetian-blind and mesh dynode structures.

6 the signal forming process at the anode

So far, we have considered the arrival time of individual charge pulses at the anode: allowing for a random distribution from a scintillator of single exponential decay time-constant and including pmt jitter, normally distribution. We now assume a characteristic pulse shape, $i(t)$, at the anode, prescribed for every current pulse initiated by a single photoelectron. Furthermore, we assume $\mathcal{E}_A = 0$ so that $q = \langle g \rangle e$ where $\langle g \rangle$ is the mean gain and e is the electronic charge.

$$i(t) = q/\tau_s \exp(-t/\tau_s) \quad \dots(9)$$

Since, according to (1), $f'(t)$ is the rate of production of photoelectrons at time t , then the number of photoelectrons produced between t and $t + dt$ is $f'(t) \cdot dt$. These make a contribution to the output at time t' , of

$$dI(t') = f'(t)dt \cdot i(t' - t)$$

where, referring to **figure 8**, t' is always $\geq t$. Integrating all contributions from decays initiated between 0 and t' we have

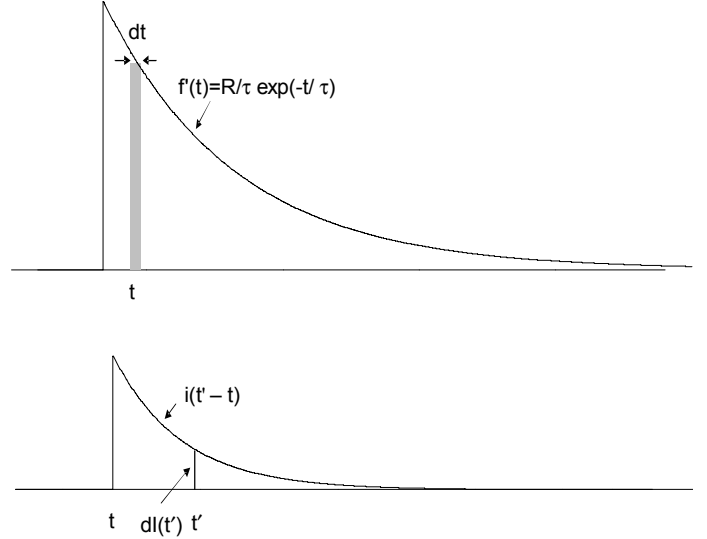


figure 8 in the signal forming process at the anode, each photoelectron produced in the time interval t to $t + dt$ contributes $dI(t')$ at time t' to the output, as shown. $I(t')$ is the sum of all such contributions from $0 < t < t'$ and is given by (10). The anode signal is negative, but in this study it is always shown positive going for convenience.

$$\begin{aligned}
 I(t') &= \int_0^{t'} R \lambda \exp(-\lambda t) \cdot q \lambda_s \exp(-\lambda_s(t' - t)) dt \\
 &= R q \lambda \lambda_s \exp(-\lambda_s t') \int_0^{t'} \exp(-(\lambda - \lambda_s)t) dt \\
 &= \frac{Rq}{(\tau - \tau_s)} [\exp(-t'/\tau) - \exp(-t'/\tau_s)] \\
 I(t) &= \frac{Rq}{(\tau - \tau_s)} [\exp(-t/\tau) - \exp(-t/\tau_s)] \quad \dots(10)
 \end{aligned}$$

replacing dummy variable t' with t .

We now generate $I(t)$ for the random emission of photons by selecting m such photons emitted at the ordered times $t_1, t_2, \dots, t_m, t_{m+1}, \dots, t_m$. We determine $\Sigma di(t') = I(t')$ at time t' contributed by the n photons emitted before t' , where $i(t')$ is given by (9). The process is much the same as that used for deriving (10) from **figure 8**. Simulations are shown in **figure 9** for $R = 500, 1000, \text{ and } 5000$.

The simulations follow the average decay curve in every case, but the noise, even for $R = 5000$, is highly significant. These simulations can be compared with actual output pulses from a detector consisting of a fast 9111B pmt (rise time 1.8 ns) and a 1" x 1" $NaI(Tl)$ crystal shown in **figure 10**. In the lower trace we can count 10 single electron pulses arriving between $t_1 = 800$ and $t_2 = 1600$ ns from the start of the event. We can estimate $R \sim 500$ from $Q = R[\exp(-\lambda t_1) - \exp(-\lambda t_2)]$.

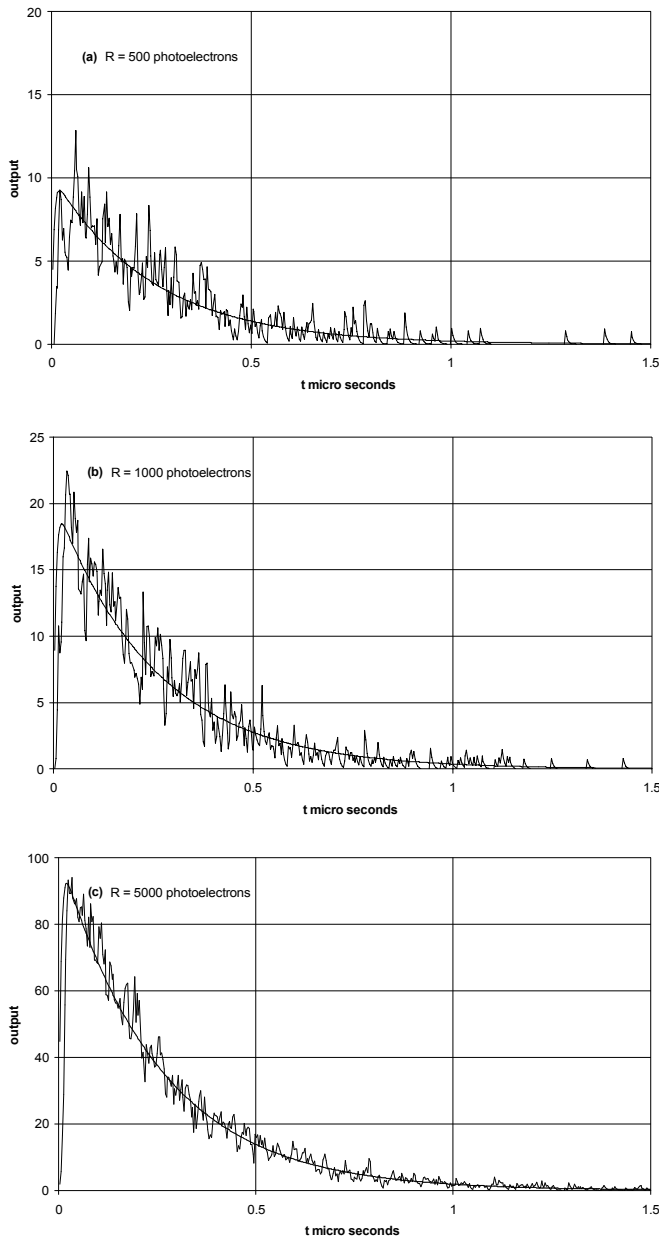


figure 9 simulated $NaI(Tl)$ decays ($\tau = 250$ ns) (a) 500 photoelectrons (b) 1000 photoelectrons and (c) 5000 photoelectrons with assumed characteristic single-electron pulse, τ_s , and jitter, ϵ_{ph} , both taken as 5 ns. The smooth curve is a plot of equation (9) without allowance for ϵ_{ph} . Note that there are still photons produced even 1.5 μ s after the initiation of the event – these pose practical problems.

6 the signal beyond the anode

In section 5 we were concerned with the current, $I(t)$, at the anode of the photomultiplier. But for practical purposes $I(t)$ must be converted into a voltage analogue. This can be done in two ways: either we connect the anode to a resistor R' with associated capacitance C' or we feed the anode directly into a transimpedance amplifier with feedback combination $R' C' = \tau_0$ [12]. The analysis and formulae are the same in both cases. The user selectable time-constant, τ_0 , has significant practical utility for smoothing spiky outputs. Referring to

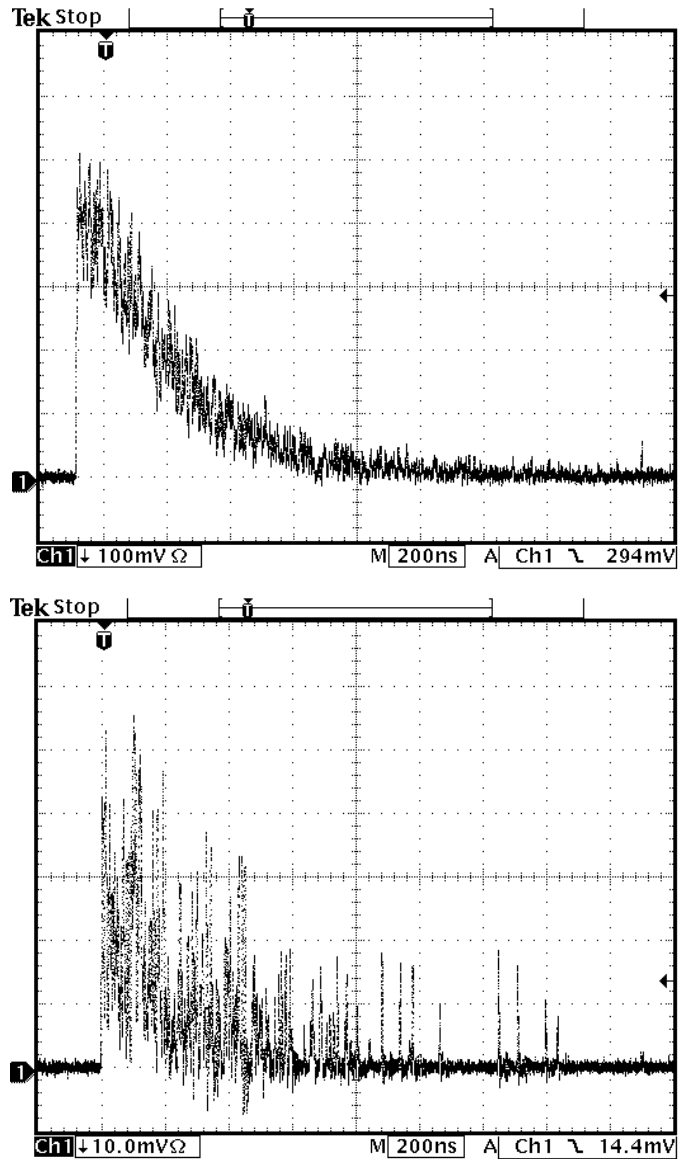


figure 10 $NaI(Tl)$ pulses measured across a 50Ω load. The upper curve contains of the order of 5000 single-electron pulses while the lower contains about 500.

the equivalent electrical circuit in **figure 11**, the output voltage, $v_0(t)$, for a stimulus $I/\tau_i \exp(-t/\tau_i)$ is [12].

$$v_0(t) = \frac{R'}{(\tau_0 - \tau_i)} (\exp(-t/\tau_i) - \exp(-t/\tau_0)) \dots (11)$$

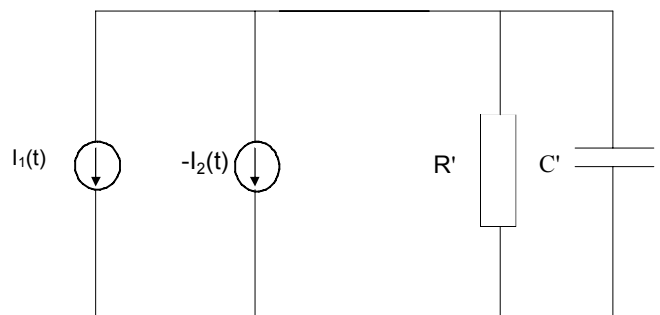


figure 11 the equivalent circuit for a photomultiplier connected to an external load R' in parallel with capacitance C' is the basis for deriving (12).

If we consider the terms in (10) as two independent

current generators, $I_1(t)$ and $-I_2(t)$ then, rearranging $I(t)$ in the following form

$$I(t) = \frac{Rq\tau}{(\tau - \tau_s)} \frac{1}{\tau} \exp(-t/\tau) - \frac{Rq\tau_s}{(\tau - \tau_s)} \frac{1}{\tau_s} \exp(-t/\tau_s)$$

we can then substitute into (11) to obtain

$$v_0(t) = \frac{R'qR}{(\tau - \tau_s)} \frac{\tau_s}{(\tau_0 - \tau)} (\exp(-t/\tau) - \exp(-t/\tau_0)) - \frac{R'qR}{(\tau - \tau_s)} \frac{\tau_s}{(\tau_0 - \tau_s)} (\exp(-t/\tau_s) - \exp(-t/\tau_0)) \dots (11)$$

Equations (10) and (12), with $R'C' = 50$ ns, are plotted in **figure 12** (c) and (d), respectively, after applying area normalisation. A Monte Carlo simulation, for $R = 100$, is shown for $I(t)$, (a), and for $v_0(t)$ in (b). The individual photon structure of the event is clearly visible in the current waveform (a) and the gap in the signal just before $0.1 \mu s$ is noteworthy. This same gap also shows up clearly in **figure 1**.

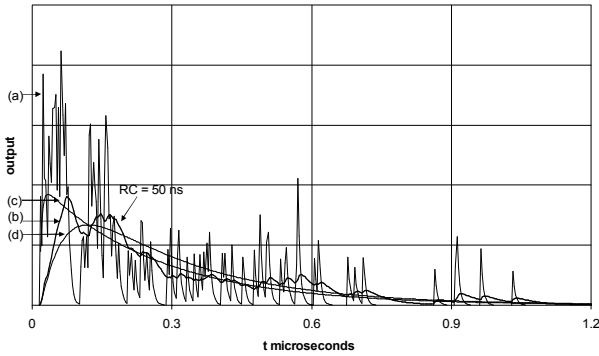


figure 12 the highly structured trace (a) is a simulation with $R = 100$, $\tau = 250$ ns, $\tau_s = 5$ ns and $\epsilon_{ph} = 5$ ns. (b) is the result of smoothing (a) with time-constant $R'C'$. (c) refers to equation (10) and the average of many repeat traces of type (a) will follow this curve. (d) is a plot of equation (12) with $R'C' = 50$ ns. Note that the area under all curves is the same.

Experimental electronics systems for fast timing are invariably based on matched 50Ω transmission line; taking the stray capacitance associated with the anode as, say, 10 pF, then $\tau_0 = 50 \times 10^{-11} = 0.5$ ns satisfies the requirement $\tau_0 \ll \tau_s$ and the voltage waveform will replicate the current waveform. If, however, we make $\tau_0 \ll \tau_s$, the voltage waveform will be smoothed to the extent that the pulse may now be described as a single one, as opposed to a series of sometimes overlapping ones. This is shown in **figure 12(b)** for $\tau_0 = 50$ ns. There are obviously difficulties in attempting to time with highly structured pulses such as (a): if the threshold is set too low, at one or two photoelectrons equivalent, the discriminator will fire several times on each event; if set too high, events will be missed and the timing will suffer. We have already seen in **figure 6**

that, after including pmt jitter, optimal timing is not obtained at $Q = 1$, but rather at some higher value of Q ; the optimal value for Q depending upon R . This is consistent with the results presented in [5] in their figure 17. This has desirable consequences, for it means that we can smooth the pmt output in the manner of **figure 12(b)**, set the threshold at a few photoelectrons equivalent, and still obtain good timing. Four simulations, all for 100 photoelectrons and $\tau_0 = 50$ ns are shown in **figure 13** giving a clear indication of the structural variation from pulse to pulse.

Timing jitter on the leading edge is clearly visible. If we time at the output level corresponding to 0.4 output units (on the y axis of **figure 13**), then inspection of the traces suggests a timing error of the order of 10 ns. This was better quantified by analysing five hundred waveform simulations resulting in the distributions of **figure 14** which refer to the arrival time for the first and tenth photoelectron in every signal. We note, for $Q = 1$, the effect of jitter is to transform the steeply falling, exponential-like distribution (thin line), ($\sigma = 2.5$ ns), to one of

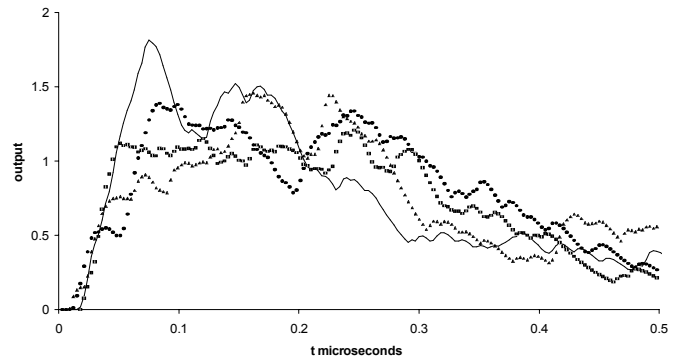


figure 13 illustrating the range of pulse shapes, all containing 100 photoelectrons. $\tau = 250$ ns, $\tau_s = \epsilon_{ph} = 5$ ns and $\tau_0 = 50$ ns. The rise times are consistent with an arrival time dispersion of 10 ns, judged by eye.

Gaussian shape with $\sigma = 4$. The actual σ ($Q=1$) for the measured distribution is 4.6 ns, as given in **figure 6(a)**. The situation for $Q = 10$ is quite different: the timing distributions for $I(t)$, $v_0(t)$ conform to the ideal shape of equation (7) and the contribution from ϵ_{ph} is barely significant. The conclusions to be drawn are profound: pmt transit-time jitter contributes significantly to overall jitter at low Q values, but its effect is considerably diluted for Q/R in excess of a few percent.

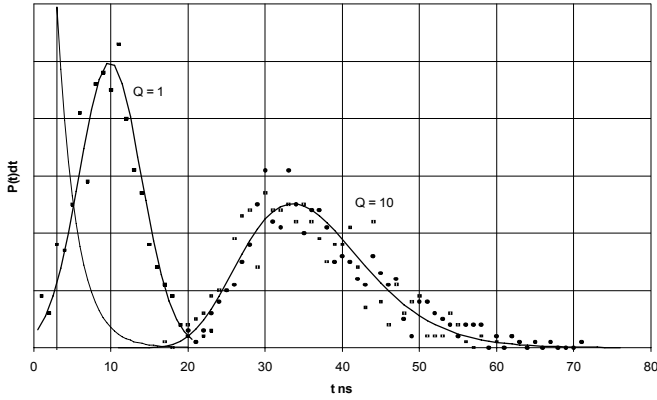


figure 14 dispersion curves for $Q = 1$ and $Q = 10$ under the same conditions as **figure 12**.

■ Monte Carlo simulation, $I(t)$, for $Q = 1$, $\sigma(Q=1) = 4.6$ may be deduced from the distribution shown. The thick solid line, for comparison, is a normal distribution with $\sigma = 4$. Note equation (7) predicts a sigma of 2.5 ns in the ideal case, $\mathcal{E}_{ph} = 0$.

This is shown by the thin line in the figure.

□ Monte Carlo simulation of $I(t)$ for $Q = 10$. $\sigma(Q=10) = 8.4$ is deduced from the distribution. Note equation (7) predicts a sigma of 7.9 ns in the ideal case, $\mathcal{E}_{ph} = 0$ (shown by the thick solid line).

● Monte Carlo simulation for $v_0(t)$ with $R'C' = 50$ ns. Here $\sigma(Q = 10) = 8.8$ ns, essentially the same value as for $I(t)$.

7 threshold and constant fraction discrimination

We learnt in section 6, with particular reference to **figure 6**, that discrimination based on the arrival of the first photoelectron does not give optimal timing when using a pmt of finite transit-time dispersion. It is fortuitous that we must set the threshold above the single photoelectron equivalent level to prevent multiple triggering on the same scintillation pulse. In so doing we may also improve timing. A well-known performance limitation with threshold discriminators is that the time at which triggering occurs depends on the amplitude of the pulse: small pulses trigger later than the larger ones. This is known as walk, but arranging to discriminate on a fixed fraction of the pulse height can eliminate it. The detector pulse is delayed and a fraction of the undelayed pulse is subtracted from it, as shown in **figure 15**.

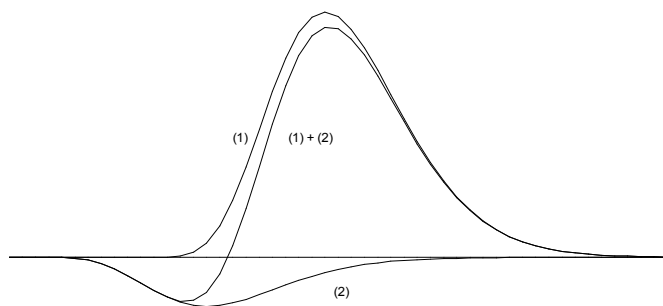


figure 15 illustrating the principle of the constant fraction discriminator. (1) is the photomultiplier output pulse and (2) is an inverted and attenuated version of (1) with 20% of the amplitude. The delay between (2) and (1) is usually taken to be equal to the rise time of the output pulse.

The time at which the composite signal crosses the time axis is amplitude independent and there are electronic circuits that can sense this point. The action of a constant fraction (CF) discriminator has been applied to one of the waveforms of **figure 13** using a delay of 50 ns and fixed fraction of 20% of pulse height with the result shown in **figure 16**. Further waveforms are given in **figure 17**: (a) refers to a δ -function SER ($NF = 1$) while for (b), the SER has $NF = 1.17$ (curve (b) of **figure 7**). The effect of noisy gain is not apparent in the degree of scatter seen in the anode waveforms, but its effect on timing dispersion is significant, as will become apparent.

Repeated waveforms of those illustrated in **figures 17** were generated. In each case, the number of photoelectrons, Q , counting from the first to arrive, to the one just past the zero-crossing time, was noted. The histograms of **figure 18** show the distributions $f(Q)dQ$ for $R = 100$ and $R = 500$. We note that $\langle Q \rangle$ is about 5 for $R = 100$ and about 23 for $R = 500$. Note, by definition of the CF process, $\langle Q \rangle$ should scale proportionately with R and the simulations show this dependence. Timing distributions are shown in **figures 19(a)** and (b) where $\mathcal{E}_{ph} = 5$ ns for various assumed SER distributions.

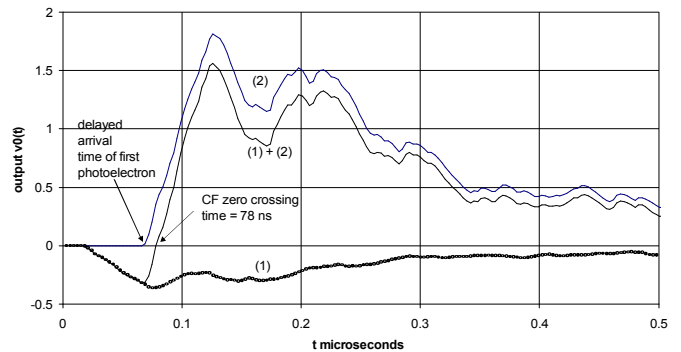


figure 16 applying the CF technique to one of the Monte Carlo waveforms of **figure 13**.

We note that the full-width at half maximum of peak height (fwhm), a figure of merit frequently quoted to characterising timing, is essentially the same for the three SER distributions. In **figure 19(a)** the fwhm is about 10 ns while in (b) it is ~ 6 ns. If we were to take the fwhm as the figure of merit for the timing dispersion then the conclusion would be that the quality of the SER is of no consequence. However, close inspection of **figure 19(a)** and (b) shows an excess of early arrivals, particularly for an exponential SER. These early arrivals (and equally any late arrivals) contribute significantly to σ while making an insignificant contribution to fwhm. Referring to **figure 18**, it is particularly clear in the histogram for $R = 500$, $\mathcal{E}_A = 0.37$ that the excess of low Q values relate to the early arrivals and that the late arrivals correspond to high Q numbers. The relationship

between σ and \mathcal{E}_A is summarised in **table 1**.

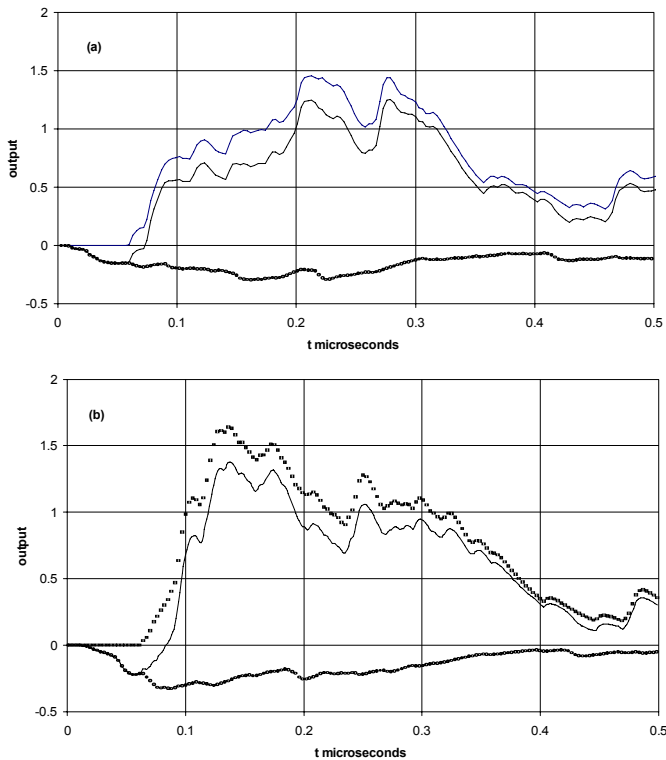


figure 17 applying the CF technique to the Monte Carlo waveforms of **figure 13**. In (a) the pmt gain is assumed noiseless ($\mathcal{E}_A = 0$) while in (b) the single-electron response of **Figure 7(b)** is assumed ($\mathcal{E}_A = 0.37$).

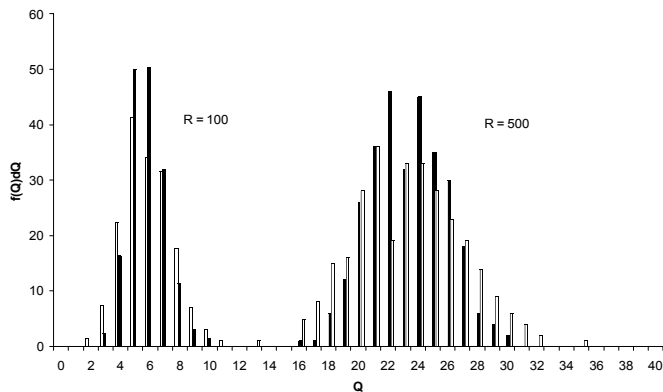


figure 18 the number of photoelectrons, Q , required to trigger a CFD (20% , 50 ns delay). ■ noiseless gain ($\mathcal{E}_A = 0$) ; □ SER taken as **figure 7(b)** ($\mathcal{E}_A = 0.37$)

table 1 summary of CF transit-time dispersion simulations for various values of \mathcal{E}_A . Note the σ values scale as $(1 + \mathcal{E}_A)^{1/2}$.

R	$\sigma(ns)$	\mathcal{E}_A	SER
100	5.15	0	δ -function
100	6.13	0.37	typical pmt
100	7.39	1.0	exponential
500	2.29	0	δ -function
500	2.89	0.37	typical pmt
500	3.16	1.0	exponential

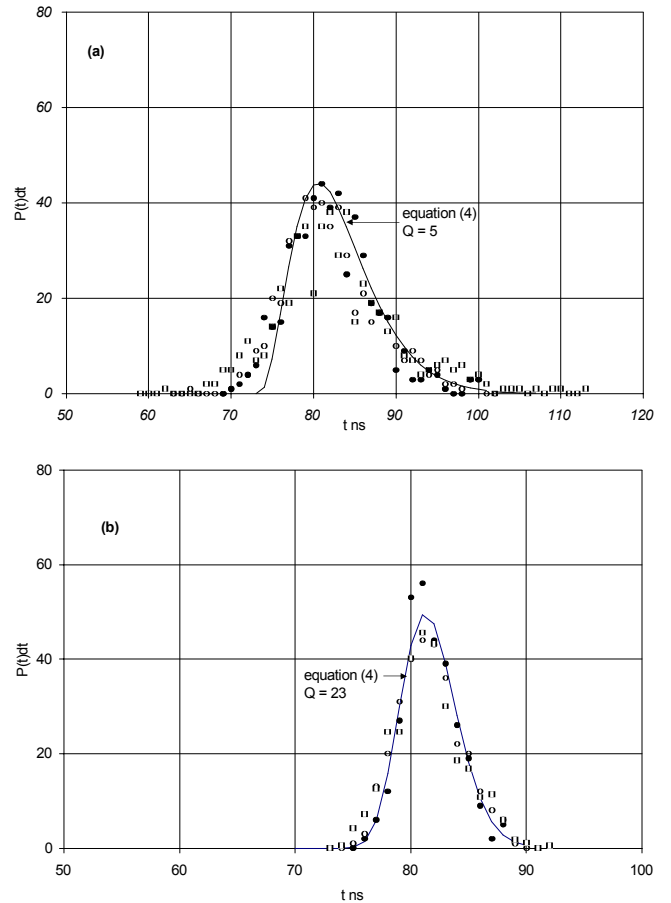


figure 19 timing distributions based on CF discrimination of 20% with 50 ns delay. ● noiseless gain ($\mathcal{E}_A = 0$); ○ SER taken as **figure 7(b)** ($\mathcal{E}_A = 0.37$) and □ exponential form for the SER ($\mathcal{E}_A = 1.0$). (a) $R = 100$, (b) $R = 500$

Note that there is no sign of walk in the two distributions of **Figures 19(a)** and (b) in accordance with the ideal concept depicted in **figure 15**.

We want to know how many photoelectrons are required to fire the constant fraction discriminator. From (12) we can determine the time at which $v_0(t)$ attains $0.2v_{max}$ for the previously assumed timing parameters. The time to reach this threshold is ~ 8 ns, which upon substitution into (2), predicts $Q/R \sim 3$. Of course this is statistical and close examination of the random arrival times in **figure 1** indicates 6 photoelectrons arrive within the first 7 ns for this particular event. The distributions in **figure 18** tell us that triggering occurs at around $Q/R = 5$ % subject to the following set-up conditions: 50 ns delay; 20% fraction and $\tau_0 = 50$ ns.

A comparison between theory and practice, as has been attempted in **figure 6(c)** for the results of [10], requires a knowledge of the mean Q/R for the particular discriminator. This is difficult to deduce with any certainty, but it is known that $\tau_0 \sim 3$ ns for the discriminator used in [10] so triggering occurs after the passage of significantly fewer photoelectrons than applies in **figure 18** - it is estimated that

$Q/R \sim 0.3\%$. There is a further uncertainty in choosing the appropriate value for R because the quality of the crystal is unknown. Taking all these uncertainties into account the best we can expect is the order of magnitude agreement apparent in **figure 6(c)**.

8 conclusions

We have seen that the treatment of [1] is useful in predicting the limit of timing performance of practical scintillation systems consisting of crystal, photomultiplier, and discriminator. This is despite the fact that [1] refers to light emission statistics only. Photomultiplier transit-time jitter, \mathcal{E}_{ph} has the effect of rearranging the time sequence of the emitted photoelectrons, and the integrated charge at the anode, at any time, t , is not necessarily due to the first Q photoelectrons. This has a compensating effect, as explained in [3], and the variance actually decreases as Q is increased from $Q = 1$ to about $Q \sim 10$ to 50 , depending on R (see **figure 6**). Some may find the dependence of $\sigma(Q)$ on \mathcal{E}_{ph} puzzling when τ is so much greater than \mathcal{E}_{ph} (considering $\tau = 250$ ns and \mathcal{E}_{ph} is only typically 1 to 5 ns).

However, as pointed out in [4], it is the initial decay rate R/τ that is the key parameter in relation to \mathcal{E}_{ph} ; at sufficiently high Q values, where the rate of emission of photoelectrons $dQ/dt \ll 1/\mathcal{E}_{ph}$, pmt jitter will be unimportant. That is why in **figure 6(a)** the influence of \mathcal{E}_{ph} is small for $R = 100$ and is negligible when $Q/R > 10\%$. The effect of \mathcal{E}_{ph} is more pronounced when $R = 5000$: it dominates \mathcal{E} at low Q and degrades the timing for Q/R up to $\sim 1\%$.

The form assumed for the single-electron response in this study, (8), is basic and thus analytically convenient. For the fast group of scintillators we will need to assume a more accurate description of the SER of the form $t^n \exp(-t/\tau_y)$, but for the present study this is not necessary and does not detract from the conclusions.

This study highlights the perhaps surprising raggedness of scintillator pulses, especially those of < 100 photoelectrons (~ 10 keV energy). The Monte Carlo simulations in the present study show considerably more structure than those of [5], primarily because they considered the case of a fast scintillator with $\tau = 3$ ns. This should sound a warning when using a scintillator with an even longer time-constant than that of $NaI(Tl)$, such as: $CsI(Tl)$, 1000 ns; $CsI(Na)$, 630 ns; BGO , 300ns; $CaF_2(Eu)$, 940 ns; $CdWO_4$, 14000

ns. With the exception of $CsI(Tl)$ they all emit less light than $NaI(Tl)$, which adds further to the raggedness. The time-constant for BGO is sufficiently close to that of $NaI(Tl)$ that the curves presented here apply, but allowance must be made for the reduced light output of BGO compared with $NaI(Tl)$.

It was mentioned in **2** that no allowance was made for the different optical paths, t_{op} , taken from emission source to photocathode. The analysis in the present study assumes $\sigma(t_{op}) \ll R/\tau$. Where this is not the case, in large area, plastic scintillation counters for example, one needs to assume a more realistic functional form of (1) derived by Monte Carlo simulation of track lengths.

The approach adopted in this study stresses the importance of visualising a pmt output signal as a superposition of R independent single-electron signals. This is the basis of **figure 8** and it is nothing other than the mathematical convolution process $f'(t) \otimes i(t)$. It is hoped that some readers will find this graphical approach beneficial. Some very elegant, but arcane, theories describing photomultiplier action have been proposed [4], [14], but the abstruse mathematical formulations seldom yield answers in simple closed form and it is interesting to note that Gatti [4], for example, ultimately resorts to the Monte Carlo approach.

Photomultiplier jitter has a major impact on timing performance, especially on the arrival time of the first single-electron pulse at the anode. It is obvious that this first pulse from an intense light flash (say $R \gg 1000$) will invariably derive from the left-hand wing of the \mathcal{E}_{ph} distribution. Clearly if R is increased there is further opportunity for the first single-electron pulse to arrive even earlier. This effect gets 'averaged out' once we consider the arrival time for the first Q single-electron pulses at the anode. This is precisely the behaviour observed in **figures 6(a) to (c)**. We note \mathcal{E}_{ph} dominates the performance until Q/R exceeds about 5 % and it has the unexpected effect of raising the optimum value of Q from 1 to a few % of R . This is beneficial for two reasons: 1) it prevents multiple triggering and 2) it advances the case for CF discriminators over threshold ones.

Gatti [3] has shown analytically that the effect of gain dispersion, \mathcal{E}_A , is to degrade \mathcal{E} by the noise factor NF , and this has been verified by simulation (see Table 1). \mathcal{E}_{ph} has exactly the same effect on timing as it does on pulse height resolution. A poor SER degrades the timing resolution by a constant factor that is independent of R . It is equiva-

lent to reducing the quantum efficiency by the same factor and it is thus a very important pmt parameter.

It is now appropriate to summarise the selection criteria for a photomultiplier, for use with a slow scintillator detecting energies in the MeV range

- high quantum efficiency
- high collection efficiency
- good single-electron response
- low transit-time jitter

The requirement for low transit-time jitter may be relaxed where low energies say below 50 keV are concerned. The remaining pmt parameters are still important.

Optimising a timing system depends on: the dynamic range required; the rate of events and on the trigger threshold. The degree of smoothing required is best established by experimentation, taking particular note of the onset of multiple triggering.

It is interesting that the CF technique has not been superseded in the forty years since its first introduction and the commercial discriminators currently available are based on the designs of the 1960s. The theory is the limitation, not the practice.

Finally, in this study the aim has been to look at the actual waveforms generated at the output of a pmt and to simulate the action of a threshold and CF discriminator on such waveforms. To the author's knowledge this has not been done previously.

references

- [1] R F Post and L I Schiff. Phys Rev.80 (1950) 1113
- [2] E Gatti and V Svelto Nucl. Instr. and Meth. 4 (1959) 189
- [3] E Gatti and V Svelto Nucl. Instr. and Meth. 30 (1964) 213
- [4] E Gatti and V Svelto Nucl. Instr. and Meth. 43 (1966) 248
- [5] L G Hyman et al Rev. Sci Instr. 35 No3, (1964) 393
- [6] D A Gedcke and W J McDonald Nucl. Instr. and Meth. 58 (1968) 253
- [7] G Ranucci. Nucl. Instr. and Meth. A 335 (1993) 121
- [8] L Janossy. Theory and practice of the evaluation of measurements. Oxford University Press, (1965), p79
- [9] F de la Barre Nucl Instr. and Meths 102 (1972) 77
- [10] R Nutt et al IEEE Trans NS 17, No 1 (1970) 299
- [11] J Braunsfurth and H J Korner Nucl. Instr. and Meths. 34 (1965) 202
- [12] A G Wright Nucl. Instr. and Meth A504 (2003) 245
- [13] W Feller. Probability theory and its applications. John Wiley, New York, (1957), p87
- [14] R Euling J Appl Phys (1963) 35, No 5,1391

appendix 1

We refer to signals at the photocathode of a pmt as photoelectrons. After amplification by the multiplier these appear at the anode still as single pulses, but they are now termed single-electron pulses. This is to stress that they originated as single-electrons although they now each contain $\langle g \rangle$ electrons.

Following Post and Shiff we refer to the total number of photons (or photoelectrons) by R . Q designates any subset of R . τ represents the time-constant of the scintillator, which, for presentational purposes is sometimes replaced by its reciprocal, λ .

The remaining terminology acknowledges the contribution of Gatti and his co-workers. R and τ refer to the same quantities, but Gatti uses C in place of Q .

$\sigma(Q)$ is the standard deviation for photoelectron statistics only

\mathcal{E}^2 is the total variance due to a combination of sources

\mathcal{E}_A^2 is the relative variance in pmt gain where $(1 + \mathcal{E}_A)$ is the gain noise factor

\mathcal{E}_{ph}^2 is the variance in the pmt transit-time jitter

τ_s is the time-constant of a single-electron pulse characterised by an exponential decay with single time-constant

τ_0 is the time-constant of an RC network connected to the anode of the pmt

appendix 2

Consider a distribution dP_t of the same form as (1)

$$dP_t = \lambda \exp(-\lambda t) dt$$

The probability of an event occurring between 0 and t is

$$P_t = \int_0^t \lambda \exp(-\lambda t) dt$$

$$P_t = 1 - \exp(-\lambda t)$$

Note that P_t is normalised since $P_{t \rightarrow \infty} = 1$ in the above.

Rearranging we have

$$t = -\tau \ln(1 - P_t)$$

We can generate a random distribution for the decay times prescribed by (1) through selecting random-numbers for P_t in the range $0 < P_t < 1$.

appendix 3

There are several points to note with respect to **figure 1**.

There are three pronounced gaps in the random events, occurring between 0 and 0.3 μs . These gaps are responsible for 'ragged' signals and pose a problem in signal encoding as discussed in section 6.

There is a tendency towards bunching, noticeably in evidence for $t > 0.5 \mu s$ and this has consequences in signal processing.

Note the random events lead from $0.05 < t < 0.3 \mu s$ and then lag between $0.3 < t < 0.55 \mu s$ and the lead only changes three or four times in 100 events. This persistent and biased deviation of the random results from the average curve is very obvious and is direct evidence against the spurious notion of 'the law of averages'. For a detailed treatment of random walks, the reader is referred to the book by Feller [13]. Figure 1 illustrates why in gambling you can't beat the banker in the long run – he can afford to wait for the lead to change, but with limited finances the gambler can't. This is not intended to trivialise the subject because in signal formation subject to random processes we have the following parallel situation: once the signal deviates significantly from the average trajectory it is unlikely to return quickly. This produces the diverse range of output waveforms even for events containing the same number of photons and subject to the same decay curve.

**talk to us about your
application or choose a product
from our literature:**

**photomultipliers, voltage dividers,
signal processing modules, housings
and power supplies**



ET Enterprises Limited
45 Riverside Way
Uxbridge UB8 2YF
United Kingdom
tel: +44 (0) 1895 200880
fax: +44 (0) 1895 270873
e-mail: sales@et-enterprises.com
web site: www.et-enterprises.com

ADIT Electron Tubes
300 Crane Street
Sweetwater TX 79556 USA
tel: (325) 235 1418
toll free: (800) 521 8382
fax: (325) 235 2872
e-mail: sales@electrontubes.com
web site: www.electrontubes.com

choose accessories for this pmt on our website

an ISO 9001 registered company

The company reserves the right to modify these designs and specifications without notice. Developmental devices are intended for evaluation and no obligation is assumed for future manufacture. While every effort is made to ensure accuracy of published information the company cannot be held responsible for errors or consequences arising therefrom.

ET Enterprises
electron tubes

© ET Enterprises Ltd, 2011
DS_ R/P099 Issue 3 (18/01/11)